Using Pseudo Transient Continuation And The Finite Element Method To Solve The Nonlinear Poisson-Boltzmann Equation

A. I. Shestakov*, J. L. Milovich**, and A. Noy***

Lawrence Livermore National Laboratory, POB 808, Livermore, CA, USA
* shestakov@llnl.gov
** milovich1@llnl.gov
*** noy1@llnl.gov

ABSTRACT

The nonlinear Poisson-Boltzmann (PB) equation is solved using Pseudo Transient Continuation. The PB solver is constructed by modifying the nonlinear diffusion module of a 3D, massively parallel, unstructured-grid, finite element, radiation-hydrodynamics code. The solver also computes the electrostatic energy and evaluates the force on a user-specified contour. Either Dirichlet or mixed boundary conditions are allowed. The latter specifies surface charges, approximates far-field conditions, or linearizes conditions "regulating" the surface charge. The code may be run in either Cartesian, cylindrical, or spherical coordinates. The potential and force due to a conical probe interacting with a flat plate is computed and the result compared with direct force measurements by chemical force microscopy.

Keywords: Poisson-Boltzmann; chemical force microscopy; pseudo transient continuation; finite elements

1 INTRODUCTION

We describe a numerical method to solve the nonlinear Poisson-Boltzmann (PB) equation and present a few examples. Space limitations preclude presenting an exhaustive list of applications of the PB equation. We refer to Israelachvili [1] for a good introduction and to Davis and McCammon [2], and Honig and Nicholls [3] for excellent reviews.

Our PB solver stems from modifying the nonlinear heat conduction (diffusion) module of the three dimensional, massively parallel, radiation-hydrodynamic code ICF3D [4] originally written to simulate inertial confinement fusion experiments. Since ICF3D discretizes spatial derivatives using the finite element method and is specifically designed for running on unstructured grids, it is uniquely suited for applications requiring high resolution in limited parts of a large computational domain. The code may be run in either Cartesian, cylindrical, or spherical coordinates. The mesh consists of an arbitrary collection of tetrahedra, pyramids, prisms, and/or hexahedra.

In the following we introduce three items pertaining to the PB theory. First, is the equation itself. Next, the related energy, and lastly, the force. Unless noted otherwise, we use CGS units.

1.1 Poisson-Boltzmann Equation

The Poisson-Boltzmann (PB) equation for the electrostatic potential V is

$$\nabla \cdot \varepsilon \nabla V + 4\pi\rho = 0 \,, \quad \rho = \rho^f + \rho^m(V) \,. \tag{1}$$

In (1), ε is the dimensionless permittivity, ρ^f is the fixed (given) charge density, and ρ^m, a function of V, simulates the mobile charge density in the solvent. If the solvent contains N types of ions, of valence Z_i, and of bulk concentration c_i (particles/cm^3), then,

$$\rho^m(V) = \sum_{i=1}^{N} c_i \, Z_i \, e \, \exp(-Z_i u) \,, \quad u \doteq eV/kT \,,$$

where e is the elementary charge, k the Boltzmann constant, and T the solvent temperature. For a symmetric 1-1 electrolyte, $N = 2$, $c_i = c_0$, and $Z_i = (-1)^i$ yielding $\rho^m = -2\, c_0\, e \, \sinh(u)$.

Boundary conditions for the PB equation are generally either of Dirichlet or of mixed type. For Dirichlet conditions, $V = V_b$ on the boundary where V_b is a given function. The mixed condition is of the form,

$$V/d + \varepsilon \, \partial V/\partial n = D_s \,, \tag{2}$$

where d and D_s are prescribed on the boundary.

Equation (2) is very useful. Setting $1/d = D_s = 0$ imposes symmetry. Setting $1/d = 0$ simulates a surface charge density $\sigma = D_s/4\pi$, while $1/d \neq 0$ and $D_s = 0$ implies that V extrapolates to zero at a distance εd. The latter choice is useful to approximate "far-field" conditions. For example, setting $1/d = \varepsilon\kappa$ and $D_s = 0$ simulates the desired $\exp(-\kappa x)$ decay in slab geometry. Lastly, if $1/d$ and D_s are both nonzero, the condition is a linearization of the "surface charge regulation condition" occurring at charged surfaces [5].

The PB equation has one important parameter, the Debye length κ^{-1}. Far away from boundaries or fixed charges, $u \ll 1$. In this limit, for an electrically neutral solvent, i.e., if $\sum c_i \, Z_i = 0$, $4\pi\,\rho^m \to -\varepsilon_s\,\kappa^2\,V$, where ε_s is the solvent permittivity,

$$\kappa^2 \doteq 4\pi(c_0 e^2/\varepsilon_s kT) \sum_{i=1}^{N} (c_i/c_0) Z_i^2 \,, \tag{3}$$

and where c_0 is a reference concentration. For a symmetric 1-1 electrolyte, $\kappa^2 = 8\pi c_0 e^2/\varepsilon_s kT$.

1.2 The Energy Integral

It can be shown that V, the solution of the PB equation, is the function which minimizes a certain functional here denoted as $W_{\rm tot}$. In the literature, the energy integral $W_{\rm tot}$ appears in different forms (Sharp and Honig [6], Overbeek [7]). Numerically, it is convenient to form $W_{\rm tot}$ from the three quantities (Zhou [8], Micu et al [9]),

$$\begin{aligned} W_f &= +(1/2)\int V\,\rho^f\,, \\ W_s &= -\int[\,\Delta\Pi + (1/2)\,V\,\rho^m\,]\,, \\ W_b &= +(1/8\pi)\oint V\,\varepsilon\,\partial V/\partial n\,. \end{aligned} \tag{4}$$

In (4), $\Delta\Pi$ denotes the excess osmotic pressure,

$$\Delta\Pi \doteq kT\sum_{i=1}^{N} c_i\,[\exp(-Z_i u) - 1]\,. \tag{5}$$

There are seemingly contradictory expressions for $W_{\rm tot}$. For example, for a 1-1 symmetric solvent, if the imposed charges are small, so is u, and since $W_s = \mathcal{O}(u^4)$, it may be neglected in computing $W_{\rm tot}$ [9]. Furthermore, if in a problem $\rho^f = 0$ and only Dirichlet boundary data is specified, then $W_{\rm tot} = -W_b$. On the other hand, if the problem only specifies a surface charge, then $W_{\rm tot} = +W_b$. This confusion is resolved by Shestakov et al [10]. Briefly, the desired functional is problem dependent and includes boundary conditions. If the problem only contains Dirichlet data, $W_{\rm tot} = W_V$ where

$$W_{\rm tot} = W_V \doteq W_f + W_s - W_b\,.$$

However, if $\sigma = \sigma_b$ is specified on the boundary, then

$$W_{\rm tot} = W_V + \oint dA\,V\,\sigma_b\,.$$

1.3 Electrostatic Force

The force between objects may be computed from the force density vector (Gilson et al [11]) which may be shown to equal the divergence of the generalized Maxwell stress tensor,

$$\mathbf{T} = \frac{\varepsilon}{4\pi}\,(\,\mathrm{E}:\mathrm{E} - \frac{1}{2}E^2\,\mathbf{I}) - \Delta\Pi\,\mathbf{I} \tag{6}$$

In (6), E^2 denotes the Euclidean norm of the electric field E ($= -\nabla V$), (E : E) is the tensor with components $(-\partial_i V)(-\partial_j V)$, $\mathbf{I}$ is the unit tensor, and $\Delta\Pi$ is given by (5). Hence, the force F over a volume $\mathcal{D}$ reduces to an integral over the enclosing surface $\partial\mathcal{D}$,

$$\mathrm{F} = \int_{\mathcal{D}} (\nabla\cdot\mathbf{T})\,d^3x = \oint_{\partial\mathcal{D}} \mathbf{T}\cdot\mathrm{dA}\,. \tag{7}$$

According to (5), $\Delta\Pi$ depends only on V, not on its gradient. However, (6) and (7) show that F depends on both V and its normal derivative at the surface. Specifically, in a cylindrically symmetric problem, the axial component of F on a flat plate located at $Z = 0$ is,

$$F_Z = (\varepsilon_s/8\pi)\,[(\partial_Z V)^2 - (\partial_R V)^2] - \Delta\Pi\,. \tag{8}$$

For an isolated plate, one for which F_Z vanishes, (8) shows that a (zero) force is due to a delicate balance between V and its derivatives on the plate. In simulations, this implies that if a boundary surface charge ($\propto \partial V/\partial n$) is specified and V is obtained by solving the PB equation, a significant fictitious force may arise unless V is computed to a high accuracy. We return to this point later, but at this time note that high surface charges imply sharp gradients, which in turn requires high accuracy of the boundary potential.

2 NUMERICAL METHOD

We now describe the algorithm use to solve (1); details are presented in [10]. Briefly, we solve the PB equation by combining Pseudo transient continuation with Newton's method. Each iteration leads to a SPD linear system which is solved using ICCG. On parallel computers, we use the ICCG variant described in [12].

However, since the solver is embedded in the code's heat conduction module, the scheme is better described in the context of solving nonlinear diffusion equations. By defining the nonlinear elliptic operator,

$$\mathcal{P}(V) \doteq \nabla\cdot\varepsilon\nabla V + 4\pi\,[\,\rho^f + \rho^m(V)\,]\,,$$

and introducing the pseudo time variable t, we note that

$$\partial V/\partial t = \mathcal{P}(V)$$

is a well posed parabolic equation whose steady state is the desired solution of the PB equation. Thus, given appropriate boundary conditions, an initial state V_0, and a time step Δt we use backward Euler differencing to (temporally) advance the solution,

$$(V - V_0)/\Delta t = \mathcal{P}(V) \tag{9}$$

where the rhs is linearized about the previous state,

$$\mathcal{P}(V) \approx \mathcal{P}(V_0) + \left.\frac{d\mathcal{P}}{dV}\right|_{V=V_0}(V - V_0)\,. \tag{10}$$

Equations (9) and (10) are discretized in space using standard finite element techniques. Second order (spatial) accuracy is guaranteed by giving the potential a "linear" representation within each cell[1].

[1] Within each cell, V has as many degrees of freedom as vertices, i.e., V is indeed linear in a tetrahedron, but trilinear in a hexahedron.

After each time step, we reset $V_0 = V$ and repeat (9) and (10) until the desired steady state is reached. Using dimensional analysis, one can estimate how long (in pseudo time) it takes to reach the steady state [10]. It is easy to show that if $\Delta t \to \infty$, (9) and (10) reduces to Newton's method. Thus, as the iterates converge, we increase Δt thereby recovering Newton's second order convergence. Initially, when we are far from the desired root, Δt is kept small and we rely on well-known stability and robustness results of implicit differencing of diffusion equations to ensure physically meaningful iterates. For reasonable meshes, our finite element discretization when combined with lumping the lower order terms leads to M-matrices. This guarantees that no new extrema are introduced by the iterates [10].

3 RESULTS

By exploiting the code's generality, we have solved a variety of PB problems, linear and nonlinear, in diverse geometries. In this section two illustrative examples are presented. (See [10] for details and other examples.) We compare the energy and potential of a charged sphere, and compute the force due to the interaction between a charged probe and a flat plate. The first simulation uses spherical coordinates; the second, cylindrical.

3.1 The Spherical Charge

Assume that a spherical ion of radius a and charge q is immersed in a symmetric 1-1 electrolyte characterized by a Debye length κ^{-1}. By Gauss' law, exterior to the ion, the potential is independent of how the (spherically symmetric) charge is distributed. Thus, it suffices to consider only the domain $r \geq a$ and on the surface of the sphere impose (2) setting $1/d = 0$ and $D_s = -q/a^2$. (At $r = r_{\max}$, we also use (2) with $1/d = \varepsilon(1 + \kappa r_{\max})/r_{\max}$ and $D_s = 0$.)

For the linearized PB equation (for which $\rho^m \propto V$), the solution is well-known [2]:

$$\begin{aligned} V &= q \exp[-\kappa(r-a)]/[r\varepsilon_s(1+\kappa a)] \,, \quad (11) \\ W_{\text{tot}} &= +W_b = q^2/[\,2a\varepsilon_s(1+\kappa a)\,] \,. \end{aligned}$$

However, if q is large (or a is small [10]), the potential of the nonlinear PB equation is appreciably smaller than that given by (11). This decrease carries over to the energy W_{tot}. We substantiate the assertions in Fig. 1 in which we compare the boundary potentials and energies of the linear and nonlinear PB equations. Curve A shows that when $q = 10e$, the nonlinear boundary potential is less than half of its linear counterpart while the energy (curve B) is reduced by nearly 40%. Curve C reflects the size of the solvent contribution to W_{tot}; when $q = 10e$, W_s accounts for nearly 25% of the energy. (For the linear PB equation, $W_s = 0$. A fact evident by noting that $\lim_{q/e \to 0} (W_b/W) = 1$.)

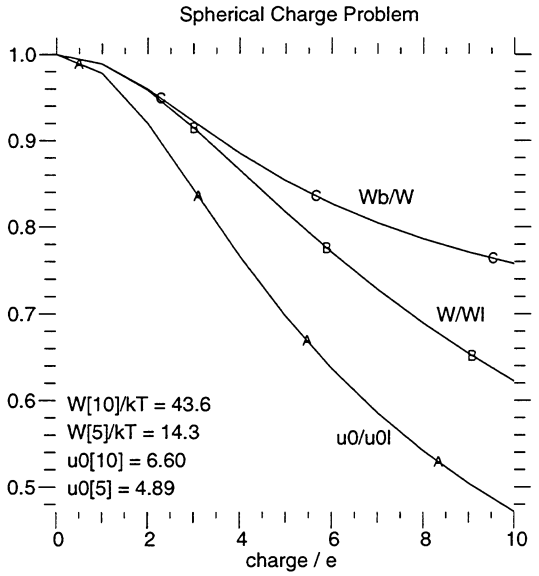

Figure 1: Comparison of linear and nonlinear results as a function of ion charge q/e. Ion radius $a = 3$ Å, Debye length $\kappa^{-1} = 4$ Å, and solvent permittivity $\varepsilon_s = 78.5$ Curve A is the ratio of the linear and nonlinear potentials at $r = a$. Curve B is the ratio of the linear and nonlinear energies $W_{\text{tot}}/W_{\text{tot},\ell}$. Curve C is the ratio W_b/W_{tot}.

3.2 Chemical Force Microscopy

We now compare experimental and computational results that measure the interaction force between a negatively charged probe and plate in an asymmetric electrolyte. The experimental procedure closely follows that of Vezenov et al [14]. Briefly, the surfaces of a gold-coated AFM probe and gold-coated silicon wafers were modified by coating them with monolayers of covalently bound 10-mercaptohexadecanoic acid (COOH). The probe and sample were immersed in a phosphate buffer solution of pH=8 and ionic strength $8.32 \cdot 10^{-4}$ M. When the probe and sample surfaces come in contact with the buffer solution, some terminal acid groups of self-assembled monolayers ionize, inducing a negative surface charge. The interaction force was measured by repeated approach-withdraw cycles. The resulting force vs. distance curve is presented in Fig. 2. Fitting the (experimental) force curve to an exponential function yields a Debye length of 8.1 nm, which is in excellent agreement with a calculated Debye length of 8.74266 nm; the latter obtained using (3), the electrolyte specification:

$$N = 4 \,, \quad Z_i = (\,-1,\, -2,\, -3,\, +1,\,) \,,$$

$$c_i/c_0 = (\,0.074595,\, 0.462668,\, 0.000023,\, 1.0\,) \,,$$

and the above stated ionic strength.

The AFM probe consists of a square pyramid tipped with a spherical cap. The pyramid's half-angle is 35°

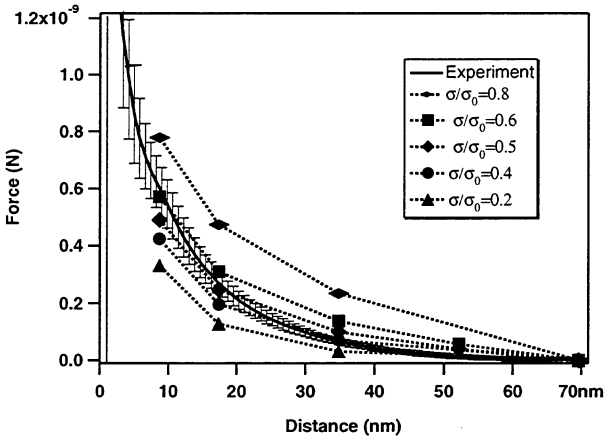

Figure 2: Chemical force microscopy, comparison of experiment and simulations. Force (nN) vs. separation distance (nm). Experimental results (solid line with error bars) was obtained by averaging over 150 separate approach-retreat cycles. Each simulation (designated by a symbol) is a separate solution of the PB equation for a particular separation distance and imposed surface charge density. The best agreement, obtained for $\sigma/\sigma_0 = 0.5$, implies that only half of the surface groups ionize.

and the cap's radius $r_p \approx 70\,\text{nm}$; the latter obtained by electron microscopy imaging. Since there is uncertainty in the magnitude of r_p, in the surface charges (see below), and in the experimental force measurement itself, we simplify the problem by assuming azimuthal symmetry and simulate the probe as a cone with a half angle $\theta_p = 38.31°$, a value which yields the same volume.

The critical parameter is the surface charge density. In the experiment, the plate and probe are coated with COOH sites whose areal number density is $1/.2\ \text{nm}^2$. Thus, if *all* the surface groups were to ionize when the probe and plate are immersed in the electrolyte, the resulting charge density would be,

$$\sigma_0 = -e/0.2\,\text{nm}^2\ . \tag{12}$$

However, the ionization of the surface groups depends on many factors. Thus, the surfaces only partially ionize. The true charge density σ is not exactly known and the value σ_0 is only an upper bound.

Because of these uncertainties, our approach is to compute the force for a series of gap distances D_{gap} and several surface charge densities,

$$\sigma/\sigma_0 = 0.1,\ 0.2,\ 0.4,\ 0.5,\ 0.6,\ 0.8 \tag{13}$$

and determine which simulation agrees with the experiment. That is, we make several calculations in which we impose

$$\varepsilon_s\, \partial V/\partial n = 4\pi\sigma \tag{14}$$

on both the probe and the plate where σ and σ_0 are given by (13) and (12) resp.

Before discussing the probe/plate interaction, we examine what happens if only the plate is immersed, or equivalently if the probe and plate lie far apart. In this regime, at the plate, we have a generalized Gouy-Chapman problem. (For the case of a 1-1 symmetric electrolyte, the analytic solution exists – see [1], [13], or [10].) For the experimental electrolyte and a choice for σ, the value of the boundary potential $\tilde{u}_b$ is found by substituting (14) into (8), ignoring $\partial_R V$ and setting the result to zero. That is, an isolated plate should feel no force. This exercise illustrates the extreme nonlinearity of the problem. Using $\sigma/\sigma_0 = 0.4$ yields $\tilde{u}_b = 10.48$, a value nearly 15 times less than the corresponding linear result, $\tilde{u}_{b,\ell} = 147.1$. For reference, $eV/kT = 10$ translates to $V \approx 8.9 \cdot 10^{-4}$ statvolt or 0.27 volt.

The nonlinearity requires high accuracy; especially at the plate surface. As mentioned above, the isolated plate feels no force only if the (computed) u_b is exact. To illustrate, we computed u_b for a generalized Gouy-Chapman problem with similar, but less nonlinear parameter settings [10] and found that if using a uniform mesh, we obtain second order convergence of u_b only with 80 cells per Debye length. Furthermore, over 1000 mesh points per Debye length are needed to just get 4 accurate decimal digits.[2] Such high resolution is, of course, unrealistic, especially in 2 or 3D runs and underscores the efficiency availed with finite elements (FE) since with FE one may adjust the mesh width to resolve large gradient regions.

The simulations require great care because of the high surface charges. If the resolution near the charged surfaces is inadequate, then an erroneous V (typically of lower magnitude) is calculated. If one simulates a configuration when the gap distance D_{gap} between the probe and plate is large, say $8\,\kappa^{-1}$, V is slightly less (in magnitude) than the exact value. If this (too low) value is then substituted into (8), F_Z turns out positive and if the expression is integrated over the plate, the result is an erroneous, positive force implying attraction. However, on physical grounds when $D_{\text{gap}} \geq 8\,\kappa^{-1}$, the force should decay to nearly zero due to the shielding. We resolve the difficulty by considering it a matter of calibration. For a given σ, we compute the force at several separations D_{gap} and declare that the true force is a difference between what we calculate and the "force" when $D_{\text{gap}} = 8\,\kappa^{-1}$ – see [10] for details.

For the simulations we typically use 240 radial cells and 480 axial cells. In the radial direction, the mesh is uniform; in the axial direction, it conforms to the boundary. At the boundaries, the axial mesh width $h_z = \mathcal{O}(10^{-5})\,\kappa^{-1}$. Results appear in Fig. 2 in which we plot the simulated force vs. distance for a number of imposed charge densities σ. We find the best agreement

[2] The chemical force microscopy simulations do indeed require such accuracy – see [10].

for $\sigma/\sigma_0 \approx 0.5 - 0.6$ implying that approximately half of the COOH groups ionize in the electrolyte.

4 SUMMARY

We have presented a numerical method to solve the nonlinear PB equation and showed its performance on two problems. Additional details and examples appear in [10]. The algorithm combines Pseudo transient continuation with Newton's method. The combination has distinct analogies with the solution of nonlinear diffusion equations. Indeed, its robustness and stability is a direct carry-over from the latter. The solver is embedded in the diffusion module of a multiphysics finite element code. Problems may be run in any of three coordinate systems and the grids can be adaptive. In fact, for more complicated PB problems, we foresee only two difficulties: mesh generation and, for very nonlinear problems, a demand for high accuracy. The former is outside the scope of this paper; entire papers, in fact separate companies, are devoted to generating grids. Meshes are input to our code in the (very general) AVS unstructured grid format. The second difficulty points to the direction of future work, viz., use higher order methods for the spatial discretization. That is, within each cell (element) represent the unknown function by higher order interpolation functions.

5 ACKNOWLEDGEMENT

This work was performed under the auspices of the U.S. Department of Energy by the University of California Lawrence Livermore National Laboratory under contract No. W-7405-Eng-48.

REFERENCES

[1] J. N. Israelachvili, *Intermolecular and Surface Forces,* 2nd edition (1992) Academic Press, London, ISBN 0-12-375181-0

[2] M. E. Davis and J. A. McCammon, "Electrostatics in Biomolecular Structure and Dynamics," *Chem Rev.*, 90, 509-521 (1990)

[3] B. Honig and A. Nicholls, "Classical Electrostatics in Biology and Chemistry," *Science,* **268**, 1144-1149, 26 May 1995

[4] A. I. Shestakov, M. K. Prasad, J. L. Milovich, N. A. Gentile, J. F. Painter, and G. Furnish, "The radiation hydrodynamic ICF3D Code," *Comput. Methods Appl. Mech. Engin.,* **187**, 181-200 (2000)

[5] E. S. Reiner and C. J. Radke, "Double Layer Interactions between Charge-regulated Colloidal Surfaces," *Adv. Colloid Interface Sci.,* **47**, 59-147 (1993)

[6] K. A. Sharp and B. Honig, "Calculating Total Electrostatic Energies with the Nonlinear Poisson-Boltzmann Equation," *J. Phys. Chem.,* **1990**, 94, 7684-7692.

[7] J. Th. G. Overbeek, "The role of energy and entropy in the electrical double layer," *Colloids Surf.,* **51**, 61-75 (1990)

[8] H.-X. Zhou, "Macromolecular electrostatic energy within the nonlinear Poisson-Boltzmann equation," *J. Chem. Phys.,* **100**, 4, 3152-3162 (1994)

[9] A. M. Micu, B. Bagheri. A. V. Ilin, L. R. Scott, and B. M. Pettitt, "Numerical Considerations in the Computation of the Electrostatic Free Energy of Interaction within the Poisson-Boltzmann Theory," *J. Comp. Phys.*, 136, 263-271 (1997)

[10] A. I. Shestakov, J. L. Milovich, and A. Noy, "Solution of the nonlinear Poisson-Boltzmann equation using Pseudo Transient Continuation and the Finite Element Method," submitted to *J. Colloid Inter. Sci.* Also available as Lawrence Livermore National Laboratory Report, UCRL-JC-139342, June 2000, Livermore, CA.

[11] M. K. Gilson, M. E. Davis, B. A. Luty, and J. A. McCammon, "Computation of Electrostatic Forces on Solvated Molecules Using the Poisson-Boltzmann Equation," *J. Phys. Chem.*, **1993**, 97, 3591-3600.

[12] A. I. Shestakov, J. L. Milovich, and D. S. Kershaw, "Parallelization of an Unstructured-grid, Laser Fusion Design Code," Applications on Advanced Architecture Computers, *siam news*, News journal of the Society for Industrial and Applied Mathematics, **32**, 3, p. 6. Also available as Lawrence Livermore National Laboratory Report UCRL-JC-133078 (1999), Livermore, CA.

[13] K. E. Forsten, R. E. Kozack, D. A. Lauffenburger, and S. Subramaniam, "Numerical Solution of the Nonlinear Poisson-Boltzmann Equation for a Membrane-Electrolyte System," *J. Phys. Chem.*, **1994**, 98, 5580-5586.

[14] D. V. Vezenov, A. Noy, L. F. Rozsnyai, and C. M. Lieber, "Force Titrations and Ionization State Sensitive Imaging of Functional Groups in Aqueous Solution by Chemical Force Microscopy," *J. Am. Chem. Soc.*, **119**, 8, 2006-2015 (1997)